ENHANCING GMAW SIMULATIONS THROUGH A HYBRID EULERIAN AND LAGRANGIAN METHOD CONSIDERING AN INCLINED WELDING TORCH

O. MOKROV*, S. WARKENTIN*, L. WESTHOFEN**, J. BENDER**, R. SHARMA*, U. REISGEN*

**RWTH Aachen University, Welding and Joining Institute, 52062 Aachen, Germany*
***RWTH Aachen University, Visual Computing Institute - LuFG Computer Animation, 52056 Aachen, Germany*
Mokrov: https://orcid.org/0000-0002-9380-6905; Warkentin: https://orcid.org/0009-0004-4514-8962;
Westhofen: https://orcid.org/0000-0003-4427-2377; Bender: https://orcid.org/0000-0002-1908-4027;
Sharma: https://orcid.org/0000-0002-6976-4530; Reisgen: https://orcid.org/0000-0003-4920-2351

DOI 10.3217/978-3-99161-089-2-003, license CC BY 4.0

ABSTRACT

The comprehensive simulation of gas metal arc welding (GMAW) remains challenging due to the continuously evolving topologies of both the welding arc region and the weld seam formation zone. GMAW involves phenomena, such as melting, hydrodynamic flows within the weld pool, and crystallization, occurring on timescales significantly distinct from the rapid plasma physics processes in the arc. This plasma exhibits pronounced heterogeneity in voltage gradients, necessitating highly precise modeling of anode and cathode layers. In contrast, traditional simulation methods couple liquid metal and arc behaviour within a single domain, typically employing Volume of Fluid (VOF) or Level Set techniques. These methods often rely on substantial simplifications in the plasma boundary layers, thereby compromising predictive accuracy. To overcome these limitations, this paper presents a hybrid modeling approach coupling a Lagrangian Smoothed Particle Hydrodynamics (SPH) model for weld pool and droplet dynamics with an Eulerian framework tailored for the arc zone. The SPH method effectively captures large-scale phenomena in the weld pool, including heat and mass transfer, droplet detachment, and solidification. On the other hand, the Eulerian model accurately represents the complex electromagnetic and thermal behaviour within the anode and cathode layers of the arc plasma

This study also addresses torch inclination effects on weld pool dynamics, heat flux distribution, and current density on the cathode, providing insights into their influence on weld geometry. Through the synthesis of both, Lagrangian and Eulerian approaches, the proposed method provides a robust tool for addressing the multiscale, multiphysics nature of the GMAW process.

Results from 3D calculations include quasi-stationary Eulerian solutions for the plasma domain and transient SPH simulation of the heat and mass transfer for a drag/push weld.

Although still under active development, this hybrid model shows significant potential for enhancing the predictive capabilities of GMAW simulations, thus offering additional possibilities in process optimization and quality improvement in industrial welding.

Keywords: simulation, modeling, GMAW, Smoothed Particle Hydrodynamics (SPH), FVM, arc plasma, push/pull weld

INTRODUCTION AND PROBLEM STATEMENT

Gas metal arc welding (GMAW) is a widely used variant of arc welding technologies. In this process, an electric arc forms between a consumable electrode (commonly poled as an anode) and the workpiece (the cathode), creating a plasma - a mixture of ionized gases, Fig. 1**.** The material from both the workpiece and the consumable wire melts, forming a shared weld pool. Upon solidification, this weld pool results in a solid weld seam. The heat required for melting the materials is generated at the sheath layers of both the anode and cathode, mainly through the recombination of ions and free electrons.

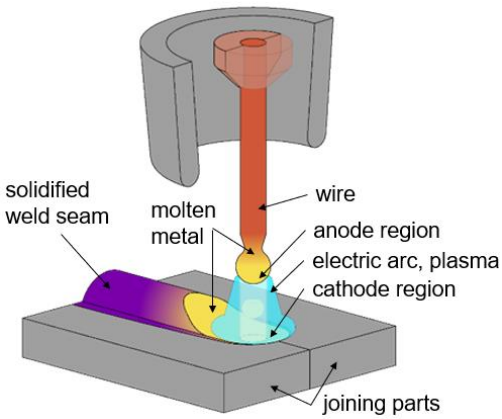

Fig. 1 Schematic representation of GMAW, illustrating the arc, anode, cathode, and weld pool regions

A key aspect of heat transfer in this process is the interaction of the arc with the anode and cathode surfaces. There is a significant feedback loop between the temperature of the molten pool surface and the physical processes occurring in the anode and cathode layers. Metal evaporation influences both the temperature of the electrodes and the composition of the plasma. Moreover, different coupling configurations alter the electric current paths, thereby affecting electromagnetic forces and heat distribution. Consequently, there is a strong interrelationship between the seam geometry and the arc, influenced by meso-scale processes in the anode and cathode regions.

The inclination of the wire also frequently plays a role, Fig. 2. In real-world welding applications, the topological changes in the process are even more pronounced. For instance,

when welding fillet welds on T-joints or lap joints, variations in plate thickness are common, which adds complexity to the weld pool behavior and seam formation. Moreover, the weld seam is often not straight, as seen in pipe welding, where the seam follows a curved path. These geometric challenges further complicate the mass and heat transfer processes, as they introduce additional variations in the melt pool dynamics and the overall heat distribution. A detailed understanding of these physical phenomena is essential for accurate modeling and remains a challenging research topic in welding simulation.

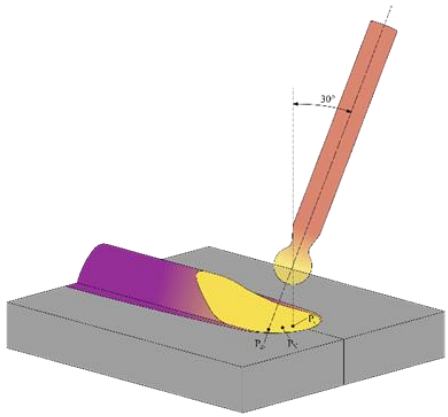

Fig. 2 Showing an inclined wire over flat plate

The scope of welding process simulation encompasses both academic and scientific questions relating to a fundamental physical understanding of the processes involved in GMAW, as well as the derivation of reference values and standards for the engineering analysis of a welded joint or structure. The decisive factor here is the determination of the temperature field in the component, which allows the mechanical and technological properties of the joint to be characterized. For this purpose, a heat source model of the welding process can be taken into account with varying degrees of abstraction and accuracy.

This study combines two approaches for simulating GMAW. Based on a preliminary analysis of the physical time scales and characteristic spatial dimensions of the corresponding physical processes, optimal numerical methods are proposed for the respective processes. Thus, the fast electromagnetic processes in the plasma are calculated using a quasi-stationary geometry of the wire and molten pool with the mesh-based FEM method, and the slower, transient processes of droplet detachment and weld seam formation are determined using a particle-based SPH solver.

HISTORICAL DEVELOPMENT AND LITERATURE REVIEW

Welding processes generate complex, time-dependent thermal fields that control the weld pool dynamics and, consequently, the final weld quality. To capture these phenomena, the classification of weld heat source models into five generations proposed by Goldak [1] offers a systematic framework for organizing welding process simulations.
It enables researchers and engineers to balance physical fidelity and computational efficiency according to the goals of the analysis. Each generation adds new physical mechanisms and mathematical complexity to the preceding one. Earlier models remain embedded as special cases in the more advanced generations.

The first generation of weld heat source models relies on highly idealized analytical descriptions, such as point, line, or plane heat sources. These models serve primarily to estimate temperature fields analytically, particularly in regions far from the weld pool. The approach simplifies heat input as a delta function and assumes steady-state conditions. While they do not account for actual energy distribution, phase changes, or nonlinear material behavior, they provide energy-conserving solutions with acceptable accuracy for far-field temperature estimates. A classic example is Rosenthal's point source model for shallow welds on thick plates [2,3].

In contrast, **second-generation** models introduce distributed energy input, replacing the delta function with volumetric or surface-based flux or temperature distributions. These models support the simulation of more complex geometries and incorporate temperature-dependent properties, boundary conditions like radiation and convection, and phase transformations. A key development is the double-ellipsoid model by Goldak, which represents power density distribution more realistically. Another important variant involves prescribed temperature distributions. However, second-generation models typically still treat the weld pool geometry as an input parameter and lack internal fluid flow descriptions [4].

Third-generation models represent a significant step forward by solving the Stefan problem, allowing for the prediction of the moving liquid-solid interface of the weld pool. These models determine the weld pool shape as part of the solution and incorporate surface forces such as arc pressure and surface tension. By coupling the heat equation with a hydrostatic momentum balance, they approximate the forces acting within a stationary liquid phase. While arc pressure and energy flux are often kept constant, the weld pool surface is computed dynamically, making these models more realistic. Weiss' extensions further included positional effects such as vertical and horizontal welding orientations [5].

Building upon this, **fourth-generation** models introduce full fluid dynamics through the solution of the Navier-Stokes equations. These models account for the complex flow phenomena within the weld pool, such as buoyancy-driven convection, Marangoni forces due to surface tension gradients, and the influence of droplet transfer. They provide a deeper insight into the internal circulation patterns of the weld pool, although they are highly nonlinear and sensitive to turbulent effects. As such, they demand greater computational resources. In practical applications, simplified or semi-empirical velocity fields - such as those developed by Sudnik - are often employed to reduce computational burden while retaining accuracy [6].

Fifth-generation models incorporate arc physics by solving the magnetohydrodynamic (MHD) equations alongside the thermal and fluid dynamic equations. These models integrate current density, electromagnetic fields, plasma properties, and their interaction with the weld pool and surrounding gas. The result is a comprehensive but extremely complex simulation framework. Due to the difficulty in ensuring numerical stability and the absence of guaranteed solution uniqueness, these models are primarily used in research settings. Nevertheless, they offer the most complete representation of arc-welding processes, including the interaction of electric arcs and molten metal in high-amperage applications with droplet transfer [7].

Table 1 Comparison of Weld Heat Source Generations.

Generation	Geometry Input	Energy Distribution	Pool Prediction	Flow	Arc Physics	Computational Time
1st	Analytical	Idealized (point/line)	NO	NO	NO	Very Low
2nd	Distributed	Realistic	Optional (input)	No	No	Low
3rd	Dynamic	Realistic	Yes (free surface)	Hydrostatic	Simplified	Moderate
4th	Dynamic	Realistic	Yes	CFD	No	High
5th	Dynamic	Realistic	Yes	Full CFD + MHD	Yes	Very High

CONCLUSION AND APPLICATION GUIDANCE

Earlier-generation models, particularly the second generation, are typically sufficient for modelling thermal behavior outside the weld pool. For detailed prediction of weld pool behavior and weld bead formation, third- or fourth-generation models are preferred.

A hierarchical or hybrid modelling strategy is strongly recommended. In this approach, different models are applied to different regions of the domain based on their physical relevance and computational demands. This modular approach simplifies the code, improves numerical robustness, and optimizes computational efficiency.

The classification proposed by Goldak et al. [1] remains a valuable framework for organizing weld heat source models and for understanding their progressive inclusion of physical mechanisms. The fifth generation, based on magnetohydrodynamic (MHD) formulations, represents the most comprehensive approach within this hierarchy, combining heat transfer, fluid flow, and electromagnetic effects. Nevertheless, these models generally treat the arc as an external energy source, neglecting the dynamic feedback between the plasma and the electrode or weld pool surface.

Recent research on

- droplet formation and detachment,
- anode sheath behavior including evaporation effects, and
- arc column models with metal vapor cores, forming a two-zone plasma characteristic of GMAW arcs,

suggests the emergence of a sixth generation of weld heat source models. In these approaches, the coupling between the arc plasma and the electrode surfaces is treated in a self-consistent manner. The models incorporate the mutual influence of plasma composition, metal vapor concentration, and surface temperature on current density and heat flux distributions. Such formulations aim to describe the entire arc–electrode–pool system as an integrated physical entity rather than a sequence of independently parameterized submodels.

Within this context, one concept stands out as particularly relevant for gas metal arc welding (GMAW) - the Evaporation Determined Arc-Cathode Coupling (EDACC) model [8]. While general sixth-generation concepts address plasma-electrode coupling in a broad sense, the EDACC model provides a dedicated formulation for GMAW, where metal evaporation from the molten pool exerts a dominant influence on arc behavior.

In GMAW, the mutual interaction between the plasma and the evaporating metal surface fundamentally determines the arc attachment, current distribution, and heat input. For this reason, the EDACC model can be regarded as a process-specific extension of the classical hierarchy - a tailored approach that captures the unique feedback mechanisms characteristic of this welding process.

EDACC MODEL

Various mechanisms contributing to cathode emission in GMAW processes have been investigated, including thermionic emission and the role of ionized metal atoms in the plasma. However, existing models often fail to describe these processes adequately. Many modern approaches are based on conditions typical for low-pressure environments or non-consumable tungsten cathodes, where evaporation effects are minimal.

In contrast, in gas metal arc welding, metal vapor and its interaction with the plasma play a dominant role. This interaction leads to lower effective cathode temperatures than expected and has a significant influence on the degree of ionization as well as on the current density distribution near the cathode [9].

To address these limitations, the Evaporation Determined Arc-Cathode Coupling (EDACC) model was developed at ISF in 2019. The model describes in detail the effects of evaporation on the cathode and demonstrates how metal evaporation modifies the local heat flux and flow dynamics. As a new physical concept, EDACC introduces a coupling principle that explicitly accounts for the influence of cold metal vapor on the plasma adjacent to the cathode.

This cooling effect is included as part of the total heat flux balance at the cathode surface:

$$q_{total} = q_{ion} - q_{em} - q_{evap} - q_{rad}, \quad (1)$$

where q_{ion} is the ion heat flux, q_{em} represents the losses due to thermionic emission, q_{evap} the heat flux associated with the evaporation and q_{rad} the radiation losses. Crucial parameter for the arc attachment and the current density distribution is an effective conductivity of the cathode sheath layer:

$$\sigma_{layer}(x) = \frac{j_{total}(x) \cdot t_{sheath}}{U_D}, \tag{2}$$

where the sheath layer t_{layer} and the voltage drop in the layer U_D are constant parameters. The results of the study show that a decrease in the degree of ionization due to the cooling effect of metal vapor can lead to a significant reduction in heat flux on the cathode surface, Fig. 3.

Simulation results obtained using the EDACC model indicate that a decrease in the degree of ionization caused by metal vapor cooling can significantly redistribute the heat flux to the cathode surface (Fig. 3). The cathode surface reaches temperatures slightly below the evaporation temperature, with a maximum heat flux observed at about 2600 K [8]. These findings were confirmed by two-color pyrometry measurements [9], shown in Fig. 4**.**

The results reveal an asymmetric arc attachment to the cathode, with maximum intensity observed along the leading edge of the molten front. This asymmetry strongly affects the heat and current transfer to the weld pool.

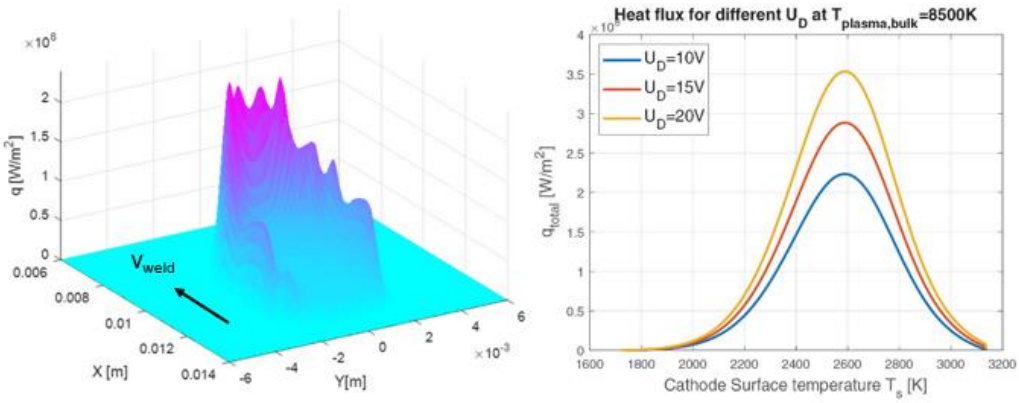

Fig. 3 Profiles illustrating heat flux distribution using the EDACC model consideration, left: crown-formed distribution pattern, right: maximal heat flux is introduced in regions below the evaporation temperature [8]

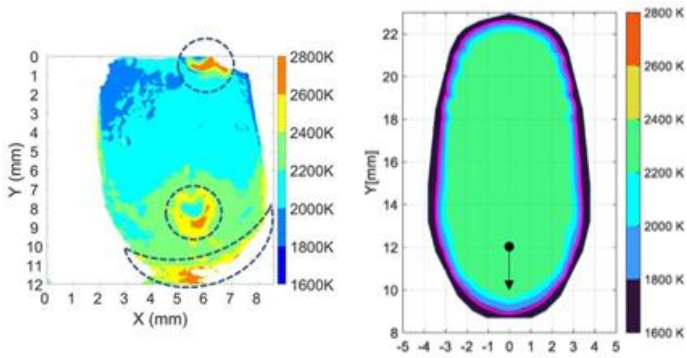

Fig. 4 Surface temperature of the melt pool, left: Measurement using two-color pyrometry (the wire (top) and its reflection on the surface of the melt pool are circled), right: Calculation result using the EDACC model [9]

In summary, the EDACC model demonstrates that a moderate amount of metal vapor is essential for stable arc attachment in GMAW processes. Excessive local evaporation, however, cools the plasma and alters the current density distribution, leading to a shift of the cathode attachment point toward less evaporated regions. This shift modifies the distributions of heat flux, current density, and Lorentz force, illustrating how evaporation from the cathode surface strongly influences all major sub-processes within GMAW models.

A further implication of this model is that the assumption of axial symmetry in the GMAW arc is a rough simplification. The spatially variable arc attachment predicted by EDACC highlights the inherently three-dimensional and transient nature of the arc–pool interaction.

THEORETICAL FOUNDATIONS OF EULERIAN GMAW MODELING

The general concept for model development divides the calculation domain in the material dependent areas: wire, arc and workpiece. Normally, wire and workpiece are of the same material. The governing equations of the process include mass (3), momentum (4) and energy conservation (5) in a general, compressible form:

$$\frac{\partial \rho}{\partial t} + \nabla \cdot (\rho \vec{v}) = 0, \tag{3}$$

$$\rho \frac{D\vec{v}}{Dt} = \rho \left(\frac{\partial v}{\partial t} + (\vec{v} \cdot \nabla)\vec{v} \right) = \rho \vec{g} - \nabla p + \nabla \cdot \bar{\bar{\tau}} + \vec{f}_L, \tag{4}$$

$$\frac{\partial \rho\, h}{\partial t} + \nabla \cdot (\rho h \vec{v}) = \nabla \cdot \left(\frac{\lambda}{c_p} \nabla h \right) + S_{Joule} + S_{Net} + S_{Sheets}, \tag{5}$$

where ρ denotes the density [kg m^{-3}], $\vec{v}$ the velocity vector [m s^{-1}], p the pressure [N m^{-2}], $\bar{\bar{\tau}}$ the viscous stress tensor [N m^{-2}], $\vec{f}_L$ the external magnetohydrodynamic, volumetric force [N m^{-3}], h the specific enthalpy [J kg^{-1}], λ the thermal conductivity [W K^{-1} m^{-1}] and the S terms represent the contribution from volumetric heat sources [W m^{-3}]. These volumetric heat

sources as well as the external volumetric force in the momentum equation (4) are introduced by adding electromagnetic considerations which lead to magnetohydrodynamics (MHD) approach. In this approach, the plasma is considered to be a continuous fluid and the problem is covered by the conductive media approximation. The electromagnetic model is coupled to the fluid flow and energy model by the consideration of the current continuity

$$\nabla \cdot \vec{j} = 0 \tag{6}$$

and the Maxwell equations. Here $\vec{j}$ is the electrical current density [A m^{-2}]. For a conductive media approximation, the electric current is connected to the electric and magnetic field by the general Ohms law:

$$\vec{j} = \sigma\,(\vec{E} + \vec{v} \times \vec{B}), \tag{7}$$

where σ is the electric conductivity [S m^{-1}], $\vec{E}$ the electric field [V m^{-1}] and $\vec{B}$ the magnet field [T].

For the consideration of the Maxwell equations an auxiliary construction using potentials is introduced. This allows for a more compact and convenient formulation of the field equations, specifically the scalar electric potential φ and the vector magnetic potential $\vec{A}$ are widely used. For the electric field $\vec{E}$ an electrical potential φ [V]is defined as

$$\vec{E} = -\nabla\varphi. \tag{8}$$

From a simplified formulation of the Ampère's Law

$$\vec{B} = \nabla \times \vec{A} \tag{9}$$

and the vector identity (with the choice of a Coulomb gauge $\nabla \cdot \vec{A} = 0$)

$$\nabla \times (\nabla \times \vec{A}) = \nabla(\nabla \cdot \vec{A}) - \nabla^2 \vec{A} \tag{10}$$

a Poisson-like transport equation for the magnetic vector potential A [V s m^{-1}] is derived:

$$\nabla^2 \vec{A} = -\mu_o \vec{j}. \tag{11}$$

The equation (9) directly relates the spatial distribution of the vector potential $\vec{A}$ to the current density $\vec{j}$. The influence of the electromagnetic field on the fluid dynamics is described by the Lorentz force $\vec{f_L}$:

$$\vec{f_L} = \vec{j} \times \vec{B}. \tag{12}$$

And the influence on the heat balance by the Joule heating S_{Joule} is described by:

$$S_{Joule} = \vec{j} \cdot \vec{E}. \tag{13}$$

Plasma radiation is usually considered as a temperature and pressure dependent material property by the kinetic calculation of a net radiation, which is included as volumetric heat loss term S_{Net}. The most challenging area in GMAW simulation is the determining of the heat source in the sheath layers, S_{Sheets} [8,10].

ADAPTIVE AND DEFORMABLE MESH TECHNIQUES

To address dynamic interfaces, adaptive mesh techniques like Arbitrary Lagrangian-Eulerian (ALE) methods and dynamic remeshing have been employed, although these approaches struggle with extensive topological changes such as droplet detachment.

These phenomena are strongly coupled to the geometries of the corresponding surfaces and require special consideration due to their complexity and the effect on both the plasma and the convection in the liquid metal. The approaches range from a simultaneous solution of the whole set of MHD equations and a dynamic resolution of the interface surfaces [11] to an assumption of quasi-stationary geometrical conditions of the molten droplet and weld pool. This assumption is justified because of the much higher reaction rate of the plasma compared to its influence on surface formation [12].

In the calculation procedure, the interface is considered as a static boundary, and the geometry of the droplet or the molten pool is updated with precalculated plasma parameters at the interface. The disadvantage of the first approach, a dynamic resolution of the interface, is a very time consuming simulation and of the second a high number of iterations for different geometric droplet and pool configuration. The decomposition of the process in quasi-stationary states delivers highly accurate values for heat flux and electric current distributions.

Nevertheless, the heat input calculation in these approaches does not consider the full spectrum of physics happening in the sheet layers. Another approach is the focus on the physics of the sheet processes for a detailed description of the phenomena on the microscopic scale. Here a detailed plasma physics calculation including species consideration is taking place. With such models the effects of the sheet processes like particle interaction, ambipolar drift, multiple ionization levels and the consideration of particle number densities are analyzed [8-10,13].

EULERIAN GRID-BASED METHODS (VOF, LEVEL SET)

The energy input distribution and electrical current distribution on the surface during the simulation of welding processes play a central role in the further evolution of the flow field and the weld shape. An important prerequisite for the numerical coupling of energy is an exact definition of the surface at which the coupling takes place. In Eulerian approaches, a phase boundary can be determined by several methods. The methods differ in the number of domains considered, with each having unique boundary conditions. For cases with two or more domains, the boundary conditions can be defined as external inputs or as interface fluxes. The motion of the boundary on a small scale can be modelled by mesh deformation. If the location of the phase boundary is not known and has to be determined the Volume of Fluid method can be used [14].

This method requires only one computational domain that includes two different fluids. The phase boundary is determined by the concentration of the mass or the distribution of the volume fraction. For this purpose, an additional transport variable is introduced in the calculations, which assigns values between 1 and 0 to the calculation cells according to the content of the medium of interest. Thus, a surface is reconstructed. Traditional Eulerian

methods such as Volume of Fluid (VOF) and Level Set were initially employed for weld simulations. Despite their ability to handle fluid interfaces, these methods face limitations due to the necessity of very fine, static meshes, particularly near regions with steep gradients.

SMOOTHED PARTICLE HYDRODYNAMICS METHOD FOR WELD POOL SIMULATION

Smoothed Particle Hydrodynamics (SPH), originally developed in astrophysics, has been adapted for welding simulations due to its inherent ability to handle topological changes without mesh adjustments. The SPH method effectively addresses challenges associated with heat and mass transfer, including droplet dynamics, thermal distribution, and solidification phenomena within the weld pool, Fig. 5**.**

In contrast to Eulerian methods that discretize the space and fix the control volumes (or grid) on a coordinate system, SPH is based on the representation of mass distribution connected to dynamically moving integration points. Thus, SPH provides significant advantages in simulating droplet dynamics and free surface flows in molten metal.

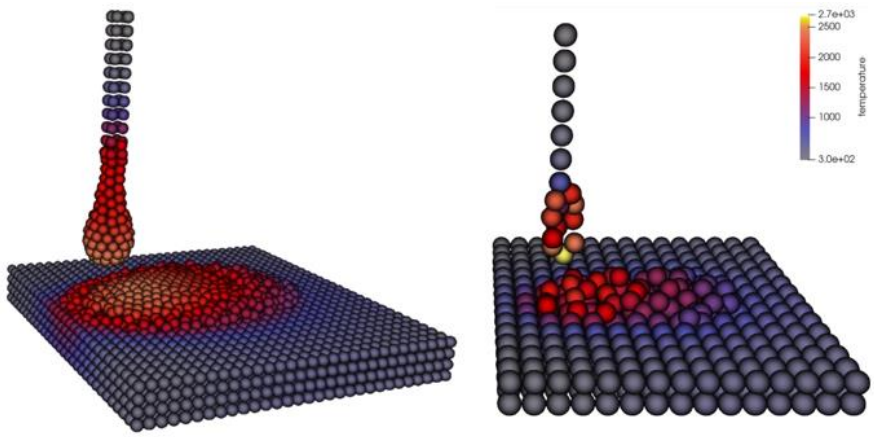

Fig. 5 Basic capabilities presentation: transient bead on plate weld simulation including heat and mass transfer, droplet detachment and phase change, wire diameter 1 mm. Left: particle radius 0.25 mm, right: particle radius 0.5 mm

SPH FOUNDATIONS

Smoothed particle hydrodynamics is a mesh-free numeric method that discretizes the continuum into a specific number of Lagrangian particles. This method, originating from astrophysics, has been adopted for fluid flow simulations and further specialized for use in welding simulations [15,16]. The discretization captures the distribution of the mass and the

advection of the mass, dynamically resolving arbitrary topology changes without prior preparation of specific regions of interest. Thus, the computational domain changes its form and boundaries according to the tracked mass distribution. In smoothed particle hydrodynamics the fluid is divided into a number of particles representing the mass included in the predefined geometry. The particles carry values of properties and field variables that are calculated depending on their position and the properties of the surrounding particles. The calculation for values stored in a particle is conducted by an interpolation inside a preset diameter around this particle. The formula for determining a variable A at the location x_i takes the following form according to a Dirac delta approximation:

$$A(x_i) \approx \sum_{j \in N_{x_i}} \frac{m_j}{\rho_j} A(x_j) W(x_i - x_j; h_{smooth}), \tag{14}$$

where m_j is the mass and ρ_j is the density at location x_j. $\mathrm{W}(x_i - x_j; h_{smooth})$ represents the kernel function with the smoothing lenght h_{smooth} and N_{x_i} the set of particles within the support radius around x_i. The particular advantage of the SPH formalism is that the gradient and divergence operators in the physical equations can be determined by applying them to the kernel:

$$\nabla A(x_i) = \sum_{j \in N_{x_i}} \frac{m_j}{\rho_j} A(x_j) \nabla_i W(x_i - x_j; h_{smooth}). \tag{15}$$

In the following, the short form W_{ij} for the kernel $\mathrm{W}(x_i - x_j; h_{smooth})$ will be used. For detailed information on the mathematical formulation of the method the reader is referred to the corresponding literature [17].

Numerous investigations have employed the incompressible smoothed particle hydrodynamics method in diverse contexts, encompassing the simulation of tungsten inert gas welding and the computation of weld pool dynamics and weld seam structure in relation to arc forces within the process [18,19]. These studies have consistently demonstrated the efficacy of the smoothed particle hydrodynamics method in accurately capturing heat transfer, non-uniform temperature fields, and weld pool dynamics influenced by numerous factors, including surface tension, Marangoni force, and arc forces [19-21].

A focus on three-dimensional modeling of thermo-mechanical responses in arc welding has emerged in several studies, highlighting the potential of mesh-free smoothed particle hydrodynamics and the coupled smoothed particle hydrodynamics with discrete element method in high-current submerged arc welding for simulating slag and weld pool formation processes [22].

Despite the demonstrated versatility and potential of the smoothed particle hydrodynamics method, existing literature underscores the necessity for ongoing research and refinement to enhance accuracy and expand its applicability. Recommendations for future research encompass the incorporation of more realistic boundary conditions and material properties, the development of increasingly accurate models for heat transfer and phase change, the exploration of alternative numerical techniques for addressing coupled thermomechanical problems, and the validation of smoothed particle hydrodynamics simulations through the utilization of experimental data [22]. Moreover, the consideration of supplementary factors

that affect weld pool dynamics and structure, such as electromagnetic fields or gas flow in welding processes, has been proposed [19]. The smoothed particle hydrodynamics method has gained significant attention in the realm of engineering applications [23] and in particular in welding simulations due to its promising results [24,25].

PHASE BOUNDARIES AND TOPOLOGY CHANGES

In particle-based smoothed particle hydrodynamics method, the surface can be determined by the so-called color function [26,27]. This function also delivers values between 1 and 0, which characterize the filling of an imaginary volume within the support radius with particles. A value of 1 means that a particle with the corresponding support radius is located in a fully dense region. The closer the particles are to the surface, the lower the values of the color function are. This is because the imaginary volume inside the support radius contains less particles in sum when moving out of the material. Numerically this concept uses the gradient of the color function resulting in the detection of the maximum gradient magnitude for the determination of the surface line. It should be noted that for both methods, Eulerian grid-based and Lagrangian particle-based, comparable concepts are used for the determination of the free surface, but with the advantage of smoothed particle hydrodynamics to use an implicit formulation. The status of the actual research shows that for a meaningful calculation of the weld seam geometry models and approaches need to be developed in order to physically describe the individual system anode, arc and cathode and to record their coupling as an overall system. In the present work the strategy is proposed to use replacement models for the processes in the anode and cathode layer based on the physics of the evaporation determined arc-cathode coupling model. By this means a compensation of the feedback through substitute models for the arc effect, both thermal and electromagnetic, is considered. The findings about the heat input distribution and current density distribution from previous work (evaporation determined arc-cathode coupling) can be integrated in smoothed particle hydrodynamics as an input boundary condition.

PROPOSED HYBRID COUPLED-DOMAIN APPROACH

To overcome individual limitations, a hybrid approach combining Eulerian grid-based arc modeling and Lagrangian SPH weld pool simulation is proposed. Data coupling strategies enable efficient exchange between domains, facilitating accurate simulations of dynamic interfaces and significant gradient regions. This hybrid model integrates evaporation determined arc-cathode coupling (EDACC) to capture the metal evaporation effects on sheath layers realistically.

The concept involves deriving an equivalent reduced substitute model for small-scale processes such as arc connection, interaction between melt surface temperature (i.e., evaporation) and plasma composition, and current density distribution from stationary FEM MHD calculations. These results will be used to create dynamic boundary conditions for the substitute models of the layer areas for the transient SPH simulation, Fig. 6.

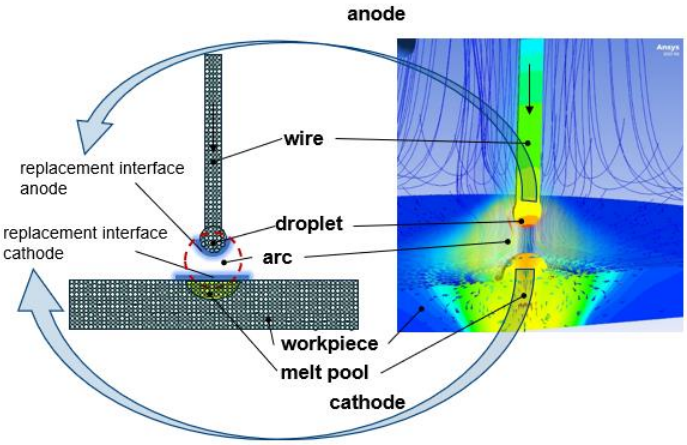

Fig. 6 Workflow of the proposed hybrid Eulerian-SPH coupling strategy

FEM 2D AXISYMMETRIC MODEL ACCORDING TO A GMAW CONFIGURATION

Firstly, a validation of the EDACC concept is conducted using a simplified geometry for an axisymmetric case. Fig. 7 shows the computational region containing three domains:

1. Argon
    a. Fluid flow
    b. Heat transfer
    c. Electric and magnetic fields
    d. Material properties: argon plasma with continuous fluid approximation 300 K-30000 K
2. Wire
    a. Heat transfer
        i. Wire feed rate considered by translational velocity for the T-field
    b. Electric and magnetic fields
    c. Material properties: S235
    d. No phase change
    e. Diameter 1 mm
    f. Tip diameter 0.5 mm
    g. Wire tip to workpiece distance 3 mm
3. Workpiece
    a. Heat transfer
    b. Fluid flow
    c. Electric and magnetic fields
    d. Material properties: S235
    e. Phase change: apparent heat capacity method

The 3 domains are thermally decoupled, 3 different variables will be solved for this task: T in argon-plasma domain, $T1$ in wire-domain and $T3$ in workpiece domain. The coupling at the cathode is established by the heat flux components of the equation (1):

$$q_{ion} = \frac{j_i}{e}\left(\frac{k_B T_e}{2} + eU_{Drop} + E_{ion} - A + \frac{H_{vap}}{N_A}\right), \tag{16}$$

$$q_{em} = \frac{j_{em}}{e}(k_B T_s + A), \tag{17}$$

$$q_{evap} = J_{vap} \cdot \frac{H_{vap}}{molar\_mass}, \tag{18}$$

$$q_{rad} = \sigma_{const}(T_s - 300\ K)^4, \tag{19}$$

where T_e is the temperature of the argon-plasma domain T and T_s the temperature in the workpiece domain $T1$. A transient calculation is conducted for a current rise from 30 A to 400 A in 0.7 s as shown in Fig. 8**.** The results show a distinct peak in current density on the cathode surface, which occurs at the edge of the melting bath, Fig. 9. The main result of this calculation is a typical temperature and velocity field in the arc and in the molten pool, but a significantly different current density distribution compared to standard models. The 2D investigations serve as an intermediate step for the construction of the 3D model and for the validation of the EDACC concept. This result is in accordance with the findings of the earlier implementations of the EDACC model.

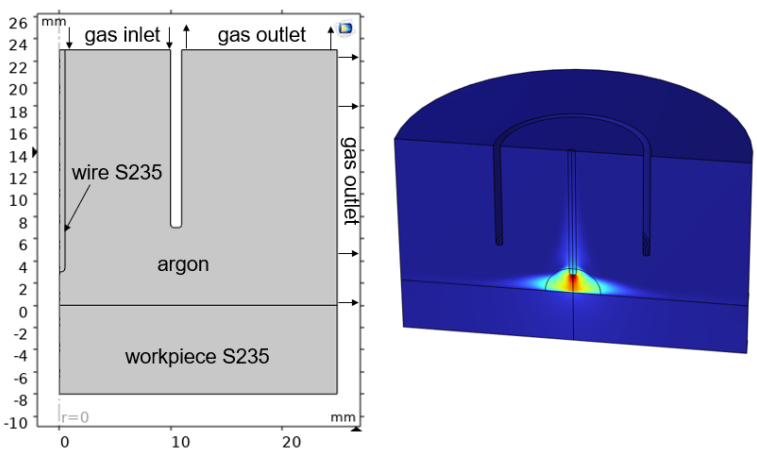

Fig. 7 2D axisymmetric computational domain. Left: domain assignment and dimensions, right: 3D representation by a 180° rotation

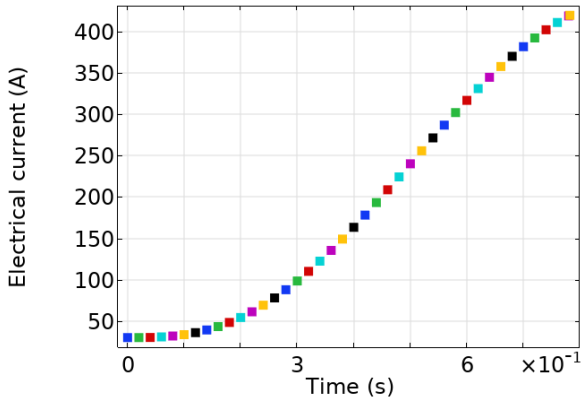

Fig. 8 Electric current ramp for the 2D axisymmetric calculation

Table 2 Process parameters

		2D, transient	3D, stationary
v_{wire}	m min^{-1}	6	6
v_{weld}	cm min^{-1}	-	50
$v_{shieldingGas}$	m s^{-1}	2	2
ETWD	mm	3	2
stickout	mm	5	8
current	A	30-400	100, 200, 300, 400
wire Ø	mm	1	1
EDACC parameter			
U_{drop}	V	3	3
t_{sheath}	mm	0.1	0.1

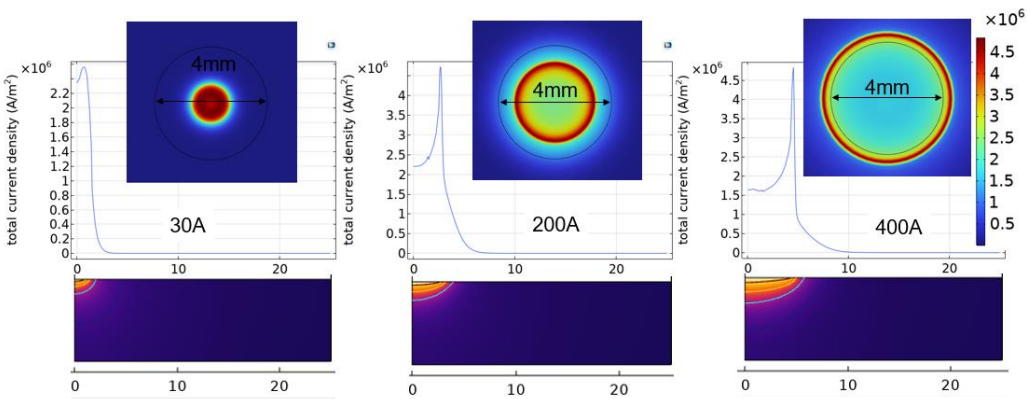

Fig. 9 Current density distribution on the cathode surface and the corresponding melt pool. Position of the current density peak is close to the melt pool edge.

FEM 3D GMAW-MODEL WITH TILTED TORCH

The goal of the investigations using a 3D model is the current density distribution with an inclined welding torch, Fig. 10. Here the same settings are used for material and computational domain definitions as for the 2D case, with the additional factor of welding speed being taken into account through a translational movement of the temperature field. Such a configuration allows for the analysis of different wire feed/welding speed and direction configurations on the same mesh, thus reducing the effort for model discretization. A stationary case is assumed for the calculation in order to set selected parameter variations.

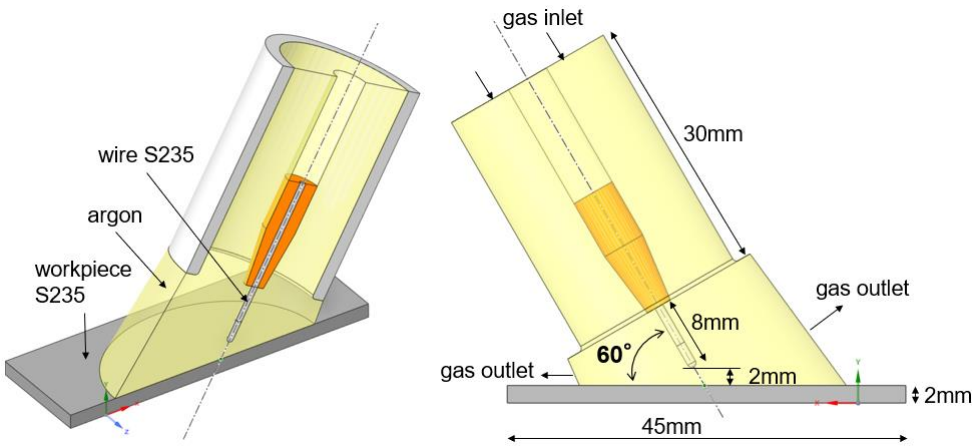

Fig. 10 3D GMAW model dimensions

3 cases were calculated: push welding, pull welding and welding with lateral inclination of the torch, Fig. 12. The selection of these configurations serves to vary the heat input on the cathode and to set different melt pool dimensions with the same electrical parameters. It should be noted here that the phase change in the workpiece is not taken into account for the 3D calculations and that the dimensions of the molten pool are analyzed on the basis of the liquidus temperature isotherms on the workpiece surface.

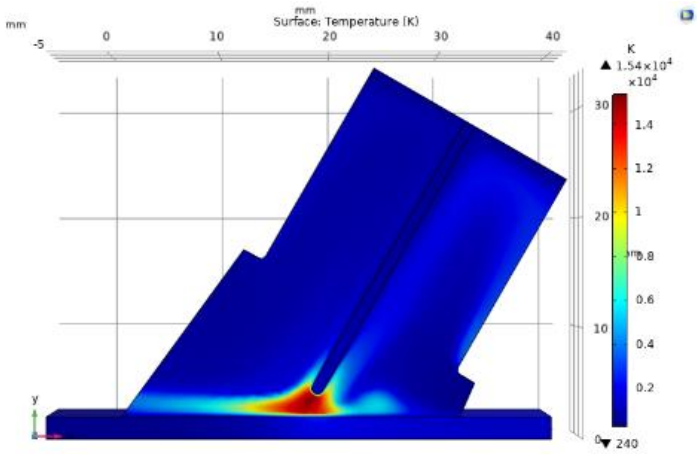

Fig. 11 Temperature distribution in a cross section view for the 100 A push welding variant

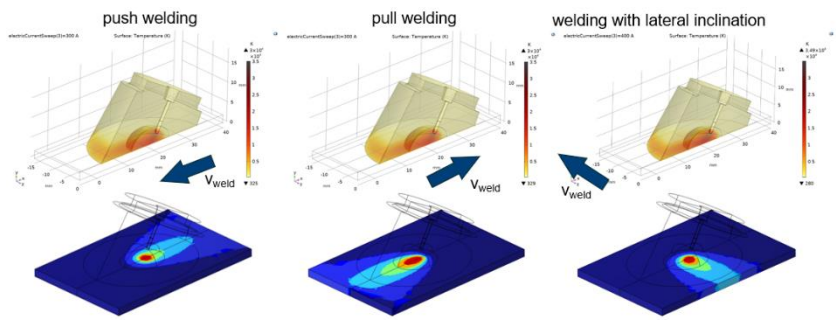

Fig. 12 Examined variants of the process arrangement

Fig. 13 illustrates the heat flux density on the cathode surface and two key observations can be made:

1. The symmetry of the heat flux density depends on the current level; at low currents, a quasi-Gaussian distribution is calculated, while at high currents, symmetry no longer applies and the distribution pattern becomes crown formed.
2. Most of the heat input occurs at the front of the molten pool, in the welding direction, where the temperature gradients are highest. This distribution is a consequence of the temperature distribution on the surface of the molten bath: the hot liquid area requires only a small amount of heat input to generate metal vapor. This vapor helps to cool the adjacent plasma, thereby reducing the conductivity of the layer. In the front, cold area of the molten bath, more energy can be absorbed (heating of the workpiece in the welding direction and, in addition, a phase change from solid to liquid), so that the conductivity limitation due to fresh metal vapor only sets in later.

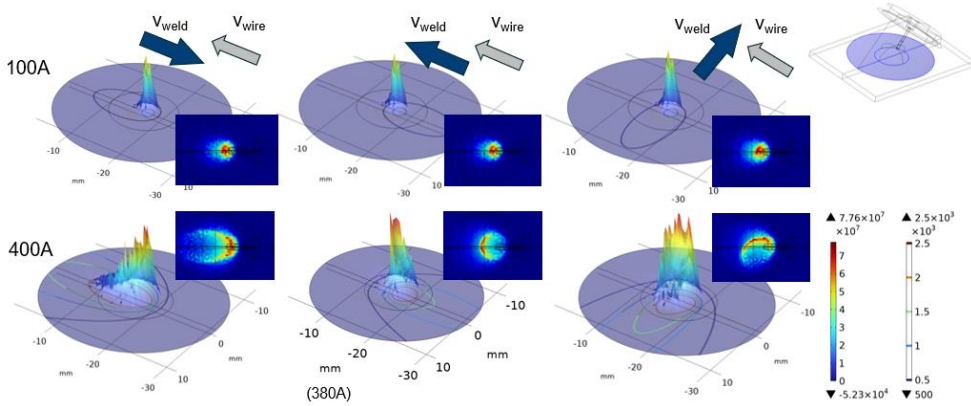

Fig. 13 Heat flux density on the cathode for 3 process arrangements and 2 electric current values. Focus: axisymmetric Gauss-like heat flux distribution for low current values and asymmetric crown-formed distribution for high current velues.

This characteristic can also be observed in the current density for the three welding configurations examined at 4 current values, with a clear pattern at high current values.

1. Push welding in Fig. 14
2. Pull welding in Fig. 15
3. Lateral welding in Fig. 16

The asymmetry of the electric current density on the cathode is particularly evident in the lateral case, Fig. 16: the burner angle has no influence on the arc connection, and no projection of the wire axis can be extrapolated for the derivation of an arc attachment pattern. Only the temperature distribution on the cathode surface allows clear conclusions to be drawn about the arc connection. A comparison of the configurations examined is shown in Fig. 17 for a current of 300 A. Based on these quasi-stationary results a replacement model for the arc connection is derived. It incorporates a temperature dependent weighting factor for the spatial distribution of the heat input.

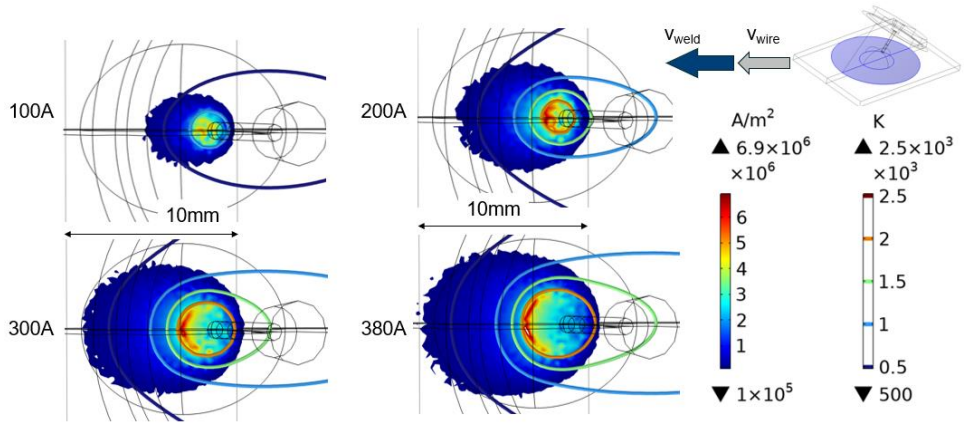

Fig. 14 Current density on the cathode at push welding configuration for 4 current values

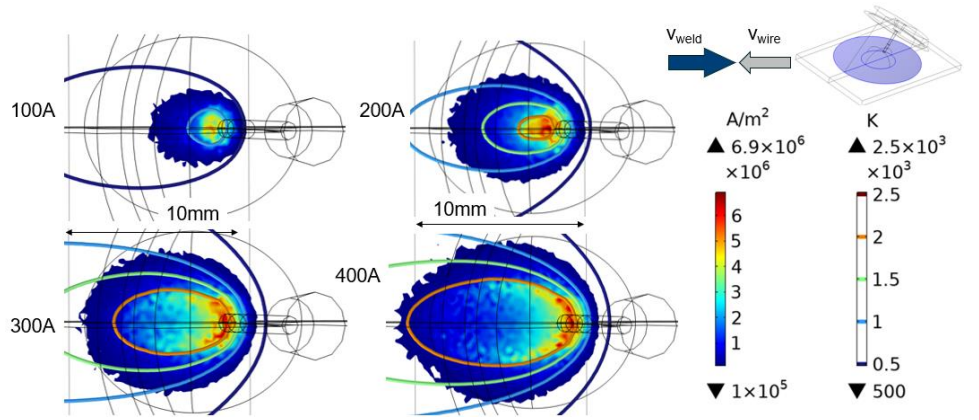

Fig. 15 Current density on the cathode at pull welding configuration for 4 current values

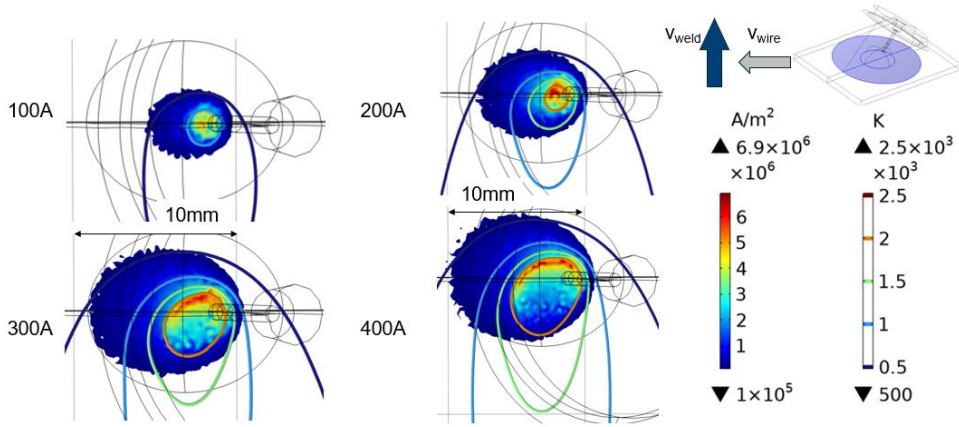

Fig. 16 Current density on the cathode at lateral welding configuration for 4 current values

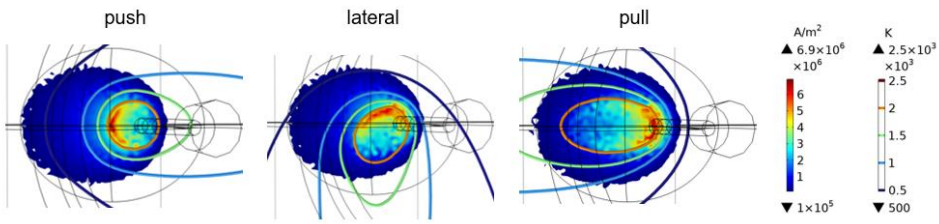

Fig. 17 Electric current density on the cathode surface for the 3 welding configurations at 300 A. Focus: arc attachment strongly depends on surface temperature distribution

SURROGATE MODEL FOR THE HEAT INPUT

The temperature dependence of the arc connection is taken into account using a cubic weighting function, equation (20). Table 3 and Fig. 18 show the parameters and the curve of the weighting function, respectively. Most of the heat is introduced in a range of $T_{evap\_offset} = 500\ \mathrm{K}$ beneath the evaporation temperature $T_{evaporation}$. The heat input near the evaporation temperature is limited by a steeply falling weighting factor in order to correspond to increased vapor formation and to represent the sharp range of the electric current density presented in Fig. 17. Towards the low temperature, the heat input is limited less strongly and distributed broadly over the surface by a low weighting factor.

Table 3 Heat distribution weighting function parameters

$T_{liquidus}$	K	1500
$T_{evaporation}$	K	2700
$T_{evaporation\_offset}$	K	500
T_{peak}	K	$T_{evaporation}$ -$T_{evaporation\_offset}$
w_{max}	-	2

$$w_h = \begin{cases} 1, & T < T_{liquidus} \\ 1 + 3x^2 - 2x^3, & T_{liquidus} < T \; and \; T < T_{peak} \\ 2 - 2(3x^2 - 2x^3), & T > T_{peak} \; and \; T < T_{evaporation} \\ 0, & T_{evap} < T \end{cases} \tag{20}$$

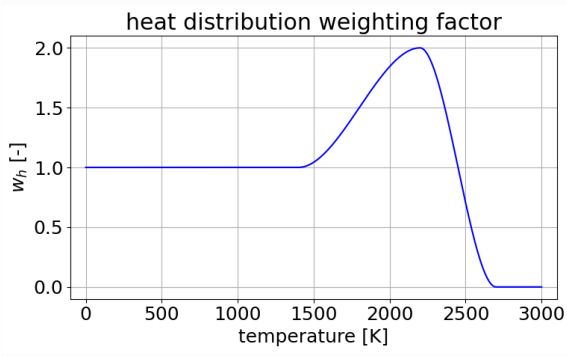

Fig. 18 Function graph for the weighting of the heat distribution

SPH-MODEL IMPLEMENTATION AND COMPUTATIONAL SETUP

This model follows the general assumptions outlined above, with restrictions due to the exclusion of temperature dependent density and electromagnetic fields in the actual implementation approach. Moreover, the model is not capable of combining fluids with high density ratios in the same computational domain. To address these constraints, the following assumptions are made:

- Electromagnetism is not directly included in the computation routine; instead, compensation models for electromagnetic effects are introduced.
- No plasma or electrical arc domain is included in the model. Compensation models for the arc effect are introduced on the corresponding surfaces.
- Evaporation (mass loss of molten metal phase) is excluded.
- Buoyant flow resulting from temperature-dependent density is not accounted for.

- Only laminar flow was considered in the melt pool. However, density is assumed constant, and thus hydrodynamics is affected only via droplet momentum.
- Limitation of a temperature maximum for consideration of evaporation loss.
- Constant radiative and convective heat transfer coefficients acting as boundary conditions on the surface.

For the material properties, a material corresponding to structural steel S235 was assumed. The material values were calculated in JMatPro according to S235 structural steel in order to cover a wide temperature range.

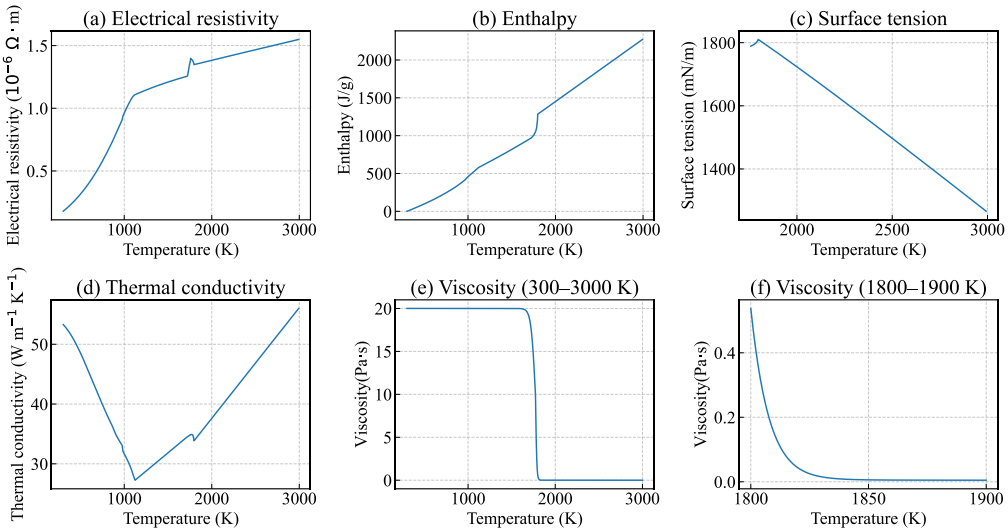

Fig. 19 Model material based on S235 steel, calculated with JMatPro

The basis for this model and the implementation of the necessary methods was carried out on a model example for tungsten inert gas welding [24]. The computational domain is divided into 3 areas: anode, arc and cathode, Fig. 6. The domains anode and cathode are directly included in the simulation, containing a mass and the according discretization by particles. The arc is not solved within the solution pipeline but is included by substitution models for the arc effects: Lorentz force, as will be described in the following section *Fluid Flow*, and heat input, as in section *Heat Transfer*.

Fluid flow

Based on the Lagrangian formulation for the continuity equation

$$\frac{D\rho}{Dt} = -\rho\nabla \cdot v, \tag{21}$$

the special case for incompressible flow is derived. Firstly, the auxiliary condition that the number of particles is set and remains constant over the simulation progress is given. Secondly, the requirement that the density always corresponds to the density at rest is postulated:

$$\rho(t) = \rho^0, \tag{22}$$

which leads to

$$\frac{D\rho_i}{Dt} = 0. \tag{23}$$

From the incompressibility constraint the divergence-freeness of the velocity field follows as well:

$$\nabla \cdot v = 0. \tag{24}$$

For the case of an incompressible flow, which is assumed in this model, the conservation of the continuity equation is achieved by reducing the velocity divergence to zero by means of balancing the pressure and pressure acceleration. The conservation of momentum for an incompressible fluid is given by the Navier–Stokes equations

$$\rho \frac{Dv}{Dt} = \rho g - \nabla p + \mu \nabla^2 v + S_L + S_{ms}. \tag{25}$$

Here, v is the velocity [m s^{-1}], p the pressure [N m^{-2}], μ the dynamic viscosity [Pa s] and the S terms represent external volumetric forces [N m^{-3}]. The change of momentum $\rho \frac{Dv}{Dt}$ is the result of acting force density fields on the right hand side, resulting in an acceleration acting on a particle:

$$a_i = \frac{Dv_i}{Dt} = \frac{f_i}{\rho_i}. \tag{26}$$

For the pressure force a symmetric formulation is used:

$$f_{pressure} = \nabla p = \sum_{j \in N_{x_i}} m_j \left(\frac{p_i}{\rho_i^2} + \frac{p_j}{\rho_j^2}\right) \nabla W_{ij}. \tag{28}$$

For an incompressible fluid, the viscous force is defined as $f_{viscosity} = \mu \nabla^2 v$. Since a standard discretization of the Laplacian is problematic because of the sign change of the second derivative of a Gaussian-like kernel the approach by Weiler et al. for a temperature dependent viscosity is chosen. [28] In this approach a combination of a SPH derivative and finite differences is used:

$$f_{viscosity} = \nabla^2 v = d \sum_{j \in N_{x_i}} \frac{m_j}{\rho_j} \frac{(v_i - v_j)(x_i - x_j)}{\|x_i - x_j\|^2 + 0.01h^2} \nabla W_{ij}, \tag{29}$$

where d is a factor representing the number of spatial dimensions and $0.01h^2$ prevents singularities.

S_L represents the Lorentz force with a classical formulation according to equation 10. In the presented model the calculation of the electromagnetic task is not included, but the effect of

the electromagnetic force. Moreover, this effect of the Lorentz force is limited to droplet detachment. No electromagnetic forces act in the molten pool. The force acting on a droplet is based on the geometric conditions of the arc. Firstly, it is assumed that this force acts only in the axial direction of the wire axis. Secondly, it is specified that the droplet is enveloped by the arc. The liquid volume (detection based on the temperature of the particles) is divided into layers with a thickness corresponding to a multiple particle diameter, Fig. 20. In accordance with the conducting wire models of [29,30] where the current lines are determined by the attachment angle of the arc, surrounding the droplet, the force is calculated in dependence of the ratio of the layer diameters to each other:

$$F_L = \frac{\mu_m \, I^2 \, log(r_{down}/r_{up})}{4\pi}. \tag{30}$$

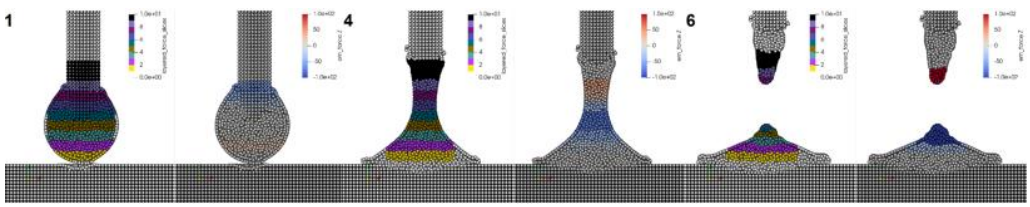

Fig. 20 Layer force model for the consideration of the Lorentz force in the SPH model. Numbers represent the time evolution in the detachment process.

In the equation (30) μ_m represents the magnetic constant (also known as the permeability of free space, $4\pi \times 10^{-7}\ N\,m^{-2}$), I the electric current [A] applied on the wire, r_{down} the mean radius of the lower layer [m] and r_{up} the mean radius of the upper layer [m]. It is obvious that F_L from equation 22 is an integral force and it is measured in Newtons. A specific force value for the corresponding layer volume is calculated from the integral force acting on a layer:

$$S_{L,i} = \frac{F_L}{\sum_{j \in layer} m_i}, \tag{31}$$

where j enumerates the number of particles in the layer and m_i a particle's mass [kg]. The model is active inside a sphere around the wire tip with a diameter of $D_{F_L} = 2 \cdot D_{wire}$. Only particles inside this sphere experience an additional acceleration that corresponds to the Lorentz force:

$$a_{i,F_L} = \frac{S_{L,i}}{\rho_i}. \tag{32}$$

S_{ms} is representing a momentum sink. During solidification materials pass through a state that is not fully liquid but also not yet solid. This condition is the so-called mushy zone. The momentum sink, also called the porosity term, is used to account for the significant reduction of momentum during the phase change process from liquid to solid. It adds a negative

acceleration to the particles in dependence of the temperature. The calculation of this term is conducted according to the procedure in the base model [24].

After summing up the individual accelerations of a particle:

$$a_i = a_{i,pressure} + a_{i,viscosity} + a_{i,F_L} + a_{i,ms}, \tag{33}$$

its velocity change

$$a_i = \frac{v_i^{t+1} - v_i^t}{\Delta t} \tag{34}$$

and thus, the position

$$v_i = \frac{x_i^{t+1} - x_i^t}{\Delta t} \tag{35}$$

is updated.

Heat transfer

In the process under consideration, the phase changes that occur (e.g. melting, solidification) should also be taken into account. As a result, enthalpy can contain a sudden change. Therefore, the classical heat conduction equation (Fourier equation)

$$\frac{\partial T}{\partial t} = \alpha \nabla^2 T, \tag{36}$$

where T is the temperature [K] and α the thermal diffusivity [$m^2\ s^{-1}$], is extended with the idea that heat conduction can also be expressed by an energy balance. The Lagrangian formulation of the Fourier equation with enthalpy is introduced for this purpose:

$$\rho \frac{Dh}{Dt} = \nabla \cdot (\lambda \nabla T) + q''', \tag{37}$$

where h denotes specific enthalpy [$J\ kg^{-1}$], ρ the material density [$kg\ m^{-3}$], T the temperature [K], λ the thermal conductivity [$W\ K^{-1}\ m^{-1}$] and q''' the contribution from volumetric heat sources [$W\ m^{-3}$]. This is particularly relevant when the process is described using an enthalpy approach in order to take into account phase changes or non-linear temperature dependencies of the specific heat. In this formulation, h considers the latent heat of melting, which is included in the temperature-dependent specific heat capacity $c_p(T)$:

$$h(T) = \int_0^T c_p(T) dT. \tag{38}$$

The heat transfer equation (29) will be discretized using smoothed particle hydrodynamics and explicit Euler time integration:

$$\rho_i \frac{h_i^{t+1} - h_i^t}{\Delta t} = \nabla \cdot (\lambda \nabla T)_i^t + q_i^{t'''}. \tag{39}$$

The discretization of the heat conduction term has the form

$$\nabla \cdot (\lambda \nabla T)_i = \sum_{j \in N_{x_i}} \frac{m_j}{\rho_j} \left(\frac{4\lambda_i \lambda_j}{\lambda_i + \lambda_j} \right) (T_i - T_j) \frac{\nabla W_{ij}}{\|x_i - x_j\|^2}. \quad (40)$$

Heat sources

The acting heat sources and sinks are summed up in the following equation:

$$q''' = q_J''' + q_A''' + w_h(T) q_C''' + q_{loss}''' \quad (41)$$

Joule heating is considered in the stick-out region (free wire length after the contact nozzle) by

$$q_J''' = \frac{1}{\sigma} j^2, \quad (42)$$

where q_J''' is the produced heat power [W m^{-3}], σ is the electric conductivity [kg^{-1} m^{-3} s^3 A^2] and j is the electrical current density [A m^{-2}]. For further SPH realization, this local power results in an energy density when multiplied with the time step. This energy is then added to the volume occupied by the discretization particle, raising its temperature. The particles are assigned to the Joule heating model using a cylinder that has a double radius of the wire. For the consideration of the heat produced in the sheath layers the surface of the anode/droplet or cathode is determined using the color function. The areas that represent an arc connection (i.e. layer areas) are then selected. This is done on the basis of a weighting with regard to the wire feed direction and the distance to the reference point in the center of the droplet. The power applied is then divided by the number of particles and divided by their volume. This results in a volumetric heat source. The distribution of the applied power occurs only to the surface particles. The arc effect in the sheath layers that heat the surfaces is based on the energy input by ionization and the material specific work function for electron emission:

$$q_{A,C}''' = j \frac{w_f}{e}, \quad (43)$$

where $q_{A,C}'''$ is the volumetric energy input at the anode or cathode [W m^{-3}], j is the electric current density [A m^{-2}], w_f is the work function [eV], $e = 1.602176634 \times 10^{-19}\ C$ is the elementary charge. It is assumed that the same material is used for both regions and a uniform current density distribution. The heat losses q_{loss}''' incorporate radiation and natural convection losses:

$$q_{rad} = \varepsilon \sigma_B (T^4 - T_0^4), \quad (44)$$

$$q_{con} = k(T - T_0), \quad (45)$$

with q_{rad} and q_{con} as surface heat losses [W m^{-2}], ε representing the material dependent emissivity factor [-], σ_B as the Stefan-Boltzmann constant 5.67×10^{-8} W m^{-2} K^{-4}, T_0 as the ambient temperature [K] and k the heat transfer coefficient [W m^{-2}].

For the application of these heat fluxes the determination of the exposed surface area is needed. Here the surface particles are also determined by the color function. The heat flux

leaving a corresponding particle is estimated with a projected cross section of a particle $A = (2r_p)^2$.

RESULTS

The presented results demonstrate the functionality and predictive capability of the developed hybrid Eulerian-SPH model. The simulations were performed for representative GMAW configurations, focusing on droplet transfer, weld pool evolution, and arc attachment behaviour under different torch orientations and process conditions.

In the hybrid framework, the Eulerian calculations provide quasi-stationary reference data for the arc plasma based on the Evaporation Determined Arc-Cathode Coupling (EDACC) model. These solutions deliver physically consistent distributions of heat flux and current density on the cathode surface, which are subsequently used as surrogate boundary models in the transient SPH simulations. Thus, the plasma-related effects - such as evaporation-driven cooling, conductivity variation, and asymmetric arc attachment - are not recalculated during the SPH computation but are incorporated through precomputed temperature-dependent substitute functions. This separation of domains ensures computational efficiency while maintaining a high degree of physical accuracy.

Fig. 21 shows the transient simulation of droplet transfer and weld pool formation. Although the case represents a relatively simple bead-on-plate configuration, all algorithms of the hybrid model are fully active, including the coupling routines for data exchange between the Eulerian and SPH domains. The influence of torch inclination and motion is dynamically included, with the welding direction intentionally set non-parallel to the plate edge. The sequence illustrates the formation, detachment, and spreading of the droplet on the substrate. The temperature field (in K) highlights localized heating of the droplet, the transient high-temperature zone upon impact, and the subsequent redistribution of thermal energy in the melt pool.

To evaluate the versatility of the SPH formulation, the model was applied to a fillet weld configuration (Fig. 22). The left image presents the raw SPH particle distribution, while the right image shows the reconstructed surface of the deposited material. This example demonstrates the robustness of the SPH method in handling complex joint geometries and multiple contact surfaces. Its mesh-free character allows a natural adaptation to evolving topologies without remeshing, an essential feature for applications such as multi-pass welding or additive manufacturing.

Finally, Fig. 23 illustrates different stages of a vertical weld with varying arc attachment patterns. The deflection of the arc connection corresponds directly to the non-uniform temperature distribution on the cathode surface. These results confirm the sensitivity of current density and heat flux distributions to local surface temperature, validating the EDACC concept and its integration via surrogate models into the hybrid framework. The sequence also demonstrates the model's ability to capture arc attachment asymmetry under realistic process conditions, including changing torch orientation and gravity effects.

Overall, the presented results confirm that the hybrid Eulerian-SPH approach successfully reproduces the essential physical mechanisms of GMAW. The combination of stationary Eulerian pre-calculations with transient SPH melt pool dynamics enables detailed yet computationally efficient modeling of the entire process chain - from arc attachment to droplet impact and solidification - through the consistent use of surrogate boundary conditions derived from physically based arc simulations.

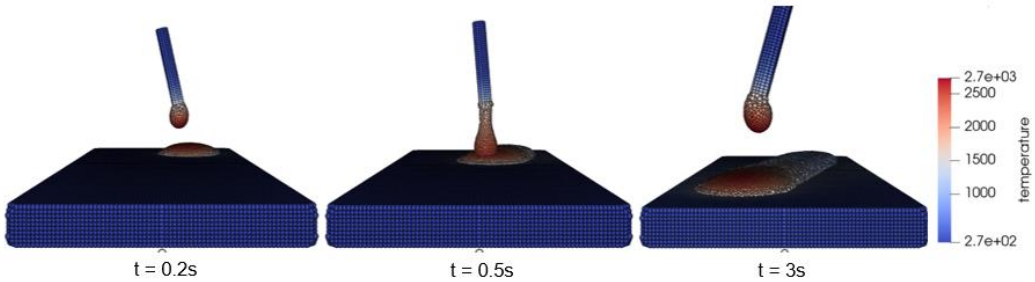

Fig. 21 SPH-based weld pool and droplet detachment dynamics incorporating thermal and flow effects. Transient simulation of droplet transfer and weld pool formation in GMAW using the hybrid Eulerian–SPH model. Although representing a relatively simple bead-on-plate case, all coupling algorithms of the hybrid model - including EDACC-based boundary conditions - are fully implemented and active. Both torch inclination and torch motion are continuously varied during the simulation, with the welding direction not aligned parallel to the plate edge. The temperature field (K) illustrates droplet detachment, impact, and spreading on the substrate.

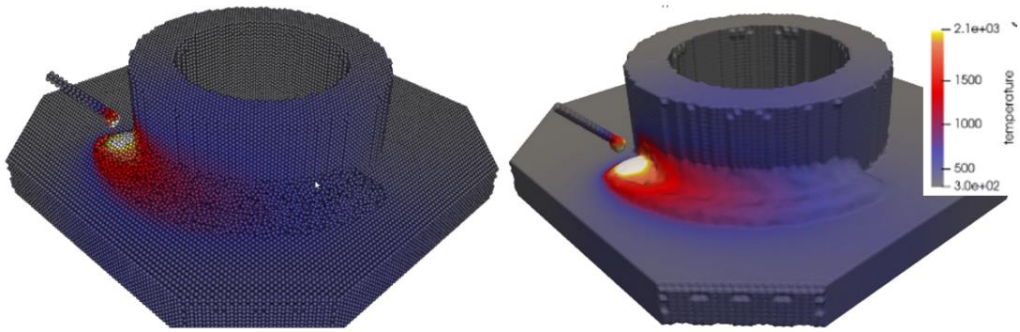

Fig. 22 Application example of a fillet weld joint modeled with the hybrid Eulerian–SPH approach. Left: raw SPH particle data; right: reconstructed surface of the deposited material. The simulation demonstrates the method's robustness in capturing complex joint geometries and boundary interactions without remeshing.

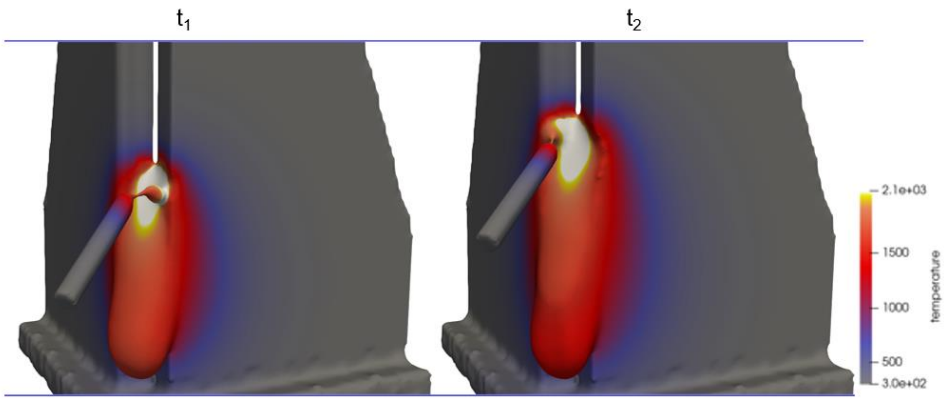

Fig. 23 Simulation of a vertical weld configuration showing the evolution of arc attachment along the cathode surface. The deflection of the arc attachment correlates with the local surface temperature distribution, confirming the asymmetric energy input predicted by the EDACC model.

DISCUSSION OF RESULTS

The results of the presented simulations clearly demonstrate the strong coupling between the melt pool surface temperature, the current density distribution, and the local heat flux within the cathode region. This coupling, as described by the Evaporation Determined Arc-Cathode Coupling (EDACC) model, leads to pronounced lateral asymmetry in current density, observed consistently across all investigated torch configurations-push, pull, and lateral inclination. The findings indicate that the commonly applied assumption of axial symmetry in two-dimensional GMAW models deviates significantly more from process reality than previously assumed.

Importantly, this asymmetry is not merely a consequence of torch geometry but an inherent physical property of the cathode sheath governed by the local temperature distribution on the melt surface. Metal vapor generated by evaporation locally cools the plasma, reducing its electrical conductivity and causing the current density peak to shift toward cooler, less evaporated regions. This behavior was clearly observed in both the quasi-stationary three-dimensional calculations and the transient two-dimensional studies.

Despite these limitations, axisymmetric two-dimensional models remain valuable for specific process domains. They can be efficiently applied to describe droplet formation and detachment in the wire region, as well as to compute the anode layer of the arc. However, for the cathode and melt pool regions - especially when the torch is in motion - such models cannot yield an acceptable representation of the heat input, since the observed asymmetry in the cathode area constitutes a native physical feature of the GMAW process.

It should also be noted that the current implementation of the EDACC-based arc model does not yet include the influence of metal vapor entering the arc plasma from the droplet surface. While this omission is not expected to qualitatively alter the main simulation

outcomes, certain quantitative effects-such as slight modifications in arc temperature distribution and local conductivity-may arise once this contribution is incorporated. The inclusion of droplet-derived vapor transport in future models will therefore be an important step toward achieving a fully self-consistent description of plasma–metal interactions in GMAW.

Beyond these aspects, the Smoothed Particle Hydrodynamics (SPH) method proves to be particularly well suited for modeling processes involving strong topological changes. Its mesh-free Lagrangian nature allows physically accurate treatment of complex and evolving geometries without remeshing. Consequently, the same modeling framework can be directly applied to welds with intricate joint configurations or to additive manufacturing processes based on wire or arc deposition, provided that appropriate process control algorithms are implemented. This highlights the natural scalability and general applicability of the proposed hybrid approach.

At the same time, it must be emphasized that welding cases dominated by strong magnetohydrodynamic (MHD) effects - such as high-current arcs or processes with significant electromagnetic feedback - the presented approach is less appropriate in its current form. In such regimes, a fully coupled MHD treatment of both plasma and liquid metal would be required to accurately capture electromagnetic interactions.

These findings provide a consistent physical interpretation of the simulation results and form the basis for developing simplified yet physically grounded boundary conditions for transient weld pool simulations. Building upon these insights, the following conclusions can be drawn.

CONCLUSION AND OUTLOOK

The presented hybrid simulation concept successfully combines the strengths of Eulerian and Lagrangian formulations for GMAW. According to the heat source classification by Goldak et al., the model merges the SPH-based concepts of the fourth generation with key elements of the sixth generation, represented by the EDACC approach. This combination enables a physically consistent description of plasma–metal interaction and provides a foundation for transient simulations of weld pool dynamics with high physical fidelity.

A particular feature of the model lies in its treatment of evaporation in the cathode region. Here, not the heat loss due to vaporization is dominant, but the resulting change in arc attachment and thus in current density distribution. This effect explains the pronounced asymmetry observed in the cathode area, which cannot be captured by axisymmetric 2D approaches. Consequently, the use of temperature-dependent surrogate functions derived from EDACC allows the asymmetric heat input to be reproduced in simplified transient SPH simulations with acceptable engineering accuracy.

In the broader process context, GMAW covers the complete material transformation cycle - from the solid state through melting and mass transfer to solidification and weld seam formation. During this evolution, thermal expansion and density variations lead to subtle topological changes that influence the joint’s thermomechanical properties. Advances in the SPH method now make it possible to capture these transitions within a unified modeling

environment, using density change as the connecting parameter between different physical stages.

Ultimately, integrating the full range of thermal, fluid, and mechanical phenomena into one consistent hybrid framework will enable a more complete description of the GMAW process, supporting predictive modeling of weld geometry, microstructure, and mechanical performance. A schematic representation of this material transformation cycle is provided in Fig. 24**,** complementing the "Heat Source Evolution" table proposed in the introduction, Table 1**.**

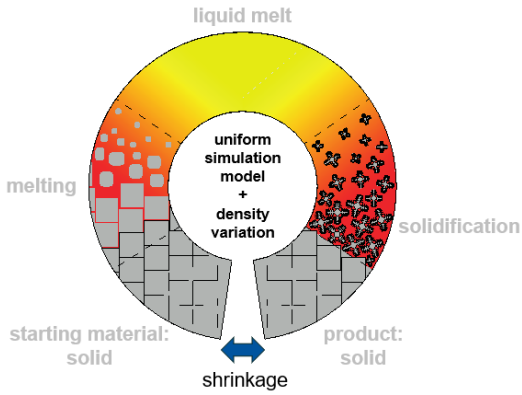

Fig. 24 Illustration of the complete material transformation cycle in GMAW, showing the interconnected physical stages of the process: heat input and melting, mass transfer and flow within the molten pool, solidification, and the development of thermomechanical properties in the final joint. The SPH method aims to capture this full cycle within a unified framework, consistent with the "Heat Source Evolution" concept presented in the introduction.

APPENDICES AND ACKNOWLEDGEMENTS

All presented investigations were conducted in the context of the Collaborative Research Centre SFB1120 "Precision Melt Engineering" at RWTH Aachen University and funded by the German Research Foundation (DFG) under the grant number 236616214. For the sponsorship and the support, we wish to express our sincere gratitude. Simulations were performed with computing resources granted by RWTH Aachen University under project rwth0398.

The authors thank Mr. Lukas Kesselburg for his contribution in programming and implementing the models used in our calculations and for the generation of analysis and rendering templates. His supervision and effort on the code maintenance have a great impact on the investigations presented in this work.

References

[1] J. A. GOLDAK and M. AKHLAGHI: *Computational Welding Mechanics*, Kluwer Academic Publishers, Boston, 2005.

[2] D. ROSENTHAL: 'Mathematical Theory of Heat Distribution During Welding and Cutting', *Welding Journal*, 20, pp. 220-234, 1941.

[3] N. N. RYKALIN: *Berechnung der Wärmevorgänge beim Schweissen*, Verlag Technik, Berlin, 1957.

[4] J. GOLDAK, A. CHAKRAVARTI and M. BIBBY: 'A new finite element model for welding heat sources', *Metallurgical Transactions B*, 15, 2, pp. 299-305, 1984.

[5] D. WEISS, K. H.CHRISTENSEN and J. K. KRISTENSEN: 'Computerized calibration of thermo-mechanical welding models', in: Horst-Hannes Cerjak, H. K. D. H. Bhadeshia, Ernst Kozeschnik (Ed.), *Mathematical Modelling of Weld Phenomena 8*, 1st ed., pp. 469-484, Verlag der Technischen Universität Graz, Graz, 2007.

[6] V. A. SUDNIK, A. V. IVANOV and W. DILTEY: 'Mathematical model of a heat source in gas-shielded consumable electrode arc welding', *Welding International*, 15, 2, pp. 146-152, 2001.

[7] S. CADIOU, M. COURTOIS, M. CARIN, W. BERCKMANS and P. LE MASSON: 'Heat transfer, fluid flow and electromagnetic model of droplets generation and melt pool behaviour for wire arc additive manufacturing', *International Journal of Heat and Mass Transfer*, 148, pp. 119102, 2020.

[8] O. MOKROV, M. SIMON, R. SHARMA and U. REISGEN: 'Arc-cathode attachment in GMA welding', *Journal of Physics D: Applied Physics*, 52, 36, pp. 364003, 2019.

[9] O. MOKROV, M. SIMON, I. SHVARTC, R. SHARMA and U. REISGEN: 'Validation of the EDACC Model for GMAW Process Simulation by Weld Pool Dimension Comparison', in: U. Reisgen et al. (Eds.), *Enhanced Material, Parts Optimization and Process Intensification*, pp. 51-59, Springer International Publishing, Cham, 2021.

[10] I. L. SEMENOV, I. V. KRIVTSUN and U. REISGEN: 'Numerical study of the anode boundary layer in atmospheric pressure arc discharges', *Journal of Physics D: Applied Physics*, 49, 10, pp. 105204, 2016.

[11] S. CADIOU, M. COURTOIS, M. CARIN, W. BERCKMANS and P. LE MASSON: '3D heat transfer, fluid flow and electromagnetic model for cold metal transfer wire arc additive manufacturing (Cmt-Waam)', *Additive Manufacturing*, 36, pp. 101541, 2020.

[12] U. REISGEN, O. MOKROV, A. ZABIROV, I. KRIVTSUN, V. DEMCHENKO, O. LISNYI and I. SEMENOV: 'Task of volumetrical evaporation and behaviour of droplets in pulsed MIG welding of AlMg alloys', *Welding in the World*, 57, 4, pp. 507-514, 2013.

[13] M. BAEVA, R. KOZAKOV, S. GORCHAKOV and D. UHRLANDT: 'Two-temperature chemically non-equilibrium modelling of transferred arcs', *Plasma Sources Science and Technology*, 21, 5, pp. 55027, 2012.

[14] A. PATHAK and M. RAESSI: 'A three-dimensional volume-of-fluid method for reconstructing and advecting three-material interfaces forming contact lines', *Journal of Computational Physics*, 307, pp. 550-573, 2016.

[15] R. A. GINGOLD and J. J. MONAGHAN: 'Smoothed particle hydrodynamics: theory and application to non-spherical stars', *Monthly Notices of the Royal Astronomical Society*, 181, 3, pp. 375-389, 1977.

[16] L. B. LUCY: 'A numerical approach to the testing of the fission hypothesis', *The Astronomical Journal*, 82, pp. 1013, 1977.

[17] D. KOSCHIER, J. BENDER, B. SOLENTHALER and M. TESCHNER: 'Smoothed Particle Hydrodynamics Techniques for the Physics Based Simulation of Fluids and Solids', https://sph-tutorial.physics-simulation.org/ (current as of Jan. 19, 2026).

[18] M. ITO, Y. NISHIO, S. IZAWA, Y. FUKUNISHI and M. SHIGETA: 'Numerical Simulation of Joining Process in a TIG Welding System Using Incompressible SPH Method', *Quarterly Journal of the Japan Welding Society*, 33, 2, pp. 34s-38s, 2015.

[19] M. TRAUTMANN, M. HERTEL and U. FÜSSEL: 'Numerical simulation of weld pool dynamics using a SPH approach', *Welding in the World*, 62, 5, pp. 1013-1020, 2018.

[20] H. KOMEN, M. SHIGETA, M. TANAKA, Y. ABE, T. FUJIMOTO, M. NAKATANI and A. B. MURPHY: 'Numerical Investigation of Heat Transfer During Submerged Arc Welding Phenomena by Coupled DEM-ISPH Simulation', *International Journal of Heat and Mass Transfer*, 171, pp. 121062, 2021.

[21] D. J. PRICE: 'Smoothed particle hydrodynamics and magnetohydrodynamics', *Journal of Computational Physics*, 231, 3, pp. 759-794, 2012.

[22] R. DAS and P. W. CLEARY: 'Novel application of the mesh-free SPH method for modelling thermo-mechanical responses in arc welding', *International Journal of Mechanics and Materials in Design*, 11, 3, pp. 337-355, 2015.

[23] K. BOBZIN, H. HEINEMANN, K. JASUTYN, S. R. JESKE, J. BENDER, S. WARKENTIN, O. MOKROV, R. SHARMA and U. REISGEN: 'Modeling the Droplet Impact on the Substrate with Surface Preparation in Thermal Spraying with SPH', *Journal of Thermal Spray Technology*, 32, 2-3, pp. 599-608, 2023.

[24] S. R. JESKE, M. S. SIMON, O. SEMENOV, J. KRUSKA, O. MOKROV, R. SHARMA, U. REISGEN and J. BENDER: 'Quantitative evaluation of SPH in TIG spot welding', *Computational Particle Mechanics*, 10, 1, pp. 1-18, 2023.

[25] O. MOKROV, S. WARKENTIN, L. WESTHOFEN, S. JESKE, J. BENDER, R. SHARMA and U. REISGEN: 'Simulation of wire metal transfer in the cold metal transfer (CMT) variant of gas metal arc welding using the smoothed particle hydrodynamics (SPH) approach', *Materialwissenschaft und Werkstofftechnik*, 55, 1, pp. 62-71, 2024.

[26] J. P. MORRIS: 'Simulating surface tension with smoothed particle hydrodynamics', *International Journal for Numerical Methods in Fluids*, 33, 3, pp. 333-353, 2000.

[27] M. MÜLLER, D. CHARYPAR and M. GROSS: *Particle-Based Fluid Simulation for Interactive Applications*, (2003).

[28] M. WEILER, D. KOSCHIER, M. BRAND and J. BENDER: 'A Physically Consistent Implicit Viscosity Solver for SPH Fluids', *Computer Graphics Forum*, 37, 2, pp. 145-155, 2018.

[29] J. C. AMSON: 'Lorentz force in the molten tip of an arc electrode', *British Journal of Applied Physics*, 16, 8, pp. 1169-1179, 1965.

[30] L. A. JONES, T. W. EAGAR and J. H. LANG: 'Magnetic forces acting on molten drops in gas metal arc welding', *Journal of Physics D: Applied Physics*, 31, 1, pp. 93-106, 1998.